THE UNIVERSITY OF ALABAMA® | University Libraries

Interlayer Exchange Coupling in Asymmetric Co-Fe/Ru/Co-Fe Trilayers Investigated with Broadband Temperature-Dependent Ferromagnetic Resonance

Tim Mewes – University of Alabama

Claudia Mewes – University of Alabama

et al.

Deposited 08/30/2018

Citation of published version:

Khodadadi, B., et al. (2017): Interlayer Exchange Coupling in Asymmetric Co-Fe/Ru/Co-Fe Trilayers Investigated with Broadband Temperature-Dependent Ferromagnetic Resonance, *Physical Review Applied 8*. https://doi.org/10.1103/PhysRevApplied.8.014024

© 2017 American Physical Society

Interlayer Exchange Coupling in Asymmetric Co-Fe/Ru/Co-Fe Trilayers Investigated with Broadband Temperature-Dependent Ferromagnetic Resonance

Behrouz Khodadadi,[1,2] Jamileh Beik Mohammadi,[1,2] Joshua Michael Jones,[1,2] Abhishek Srivastava,[1,2] Claudia Mewes,[1,2] Tim Mewes,[1,2] and Christian Kaiser[3]

[1]*Department of Physics and Astronomy, The University of Alabama, Tuscaloosa, Alabama 35487, USA*
[2]*Center for Materials for Information Technology (MINT), The University of Alabama, Tuscaloosa, Alabama 35487, USA*
[3]*Western Digital, 44100 Osgood Road, Fremont, California 94539, USA*

(Received 15 January 2017; revised manuscript received 13 May 2017; published 24 July 2017)

We report on a comprehensive study of the interlayer exchange coupling in Co-Fe(5 nm)/Ru(t)/Co-Fe(8 nm) trilayers ($t = 0.8, \ldots, 2.8$ nm) using broadband ferromagnetic resonance. A systematic frequency dependence of the field separation between the acoustic and optic modes is found, which is caused by different effective magnetizations of the two ferromagnetic layers. Hence, it is shown that the broadband measurements are vital for reducing the systematic error margins in the determination of interlayer exchange coupling using ferromagnetic resonance. We also investigate the temperature dependence of the interlayer exchange coupling and compare our results with existing theories. It is shown that models which take into account the temperature dependence due to thermal excitations of spin waves within the ferromagnetic layers have a considerably better agreement with the experiment than models solely based on spacer and interface contributions to the temperature dependence.

DOI: 10.1103/PhysRevApplied.8.014024

I. INTRODUCTION

Over the last decades, there have been extensive experimental and theoretical studies of interlayer exchange-coupled (IEC) systems consisting of two ferromagnetic layers coupled through a nonmagnetic spacer layer [1–4]. Different theoretical models have been developed to explain the oscillatory behavior based on the characteristics of the Fermi surface of the spacer layer [5,6] or using the spin-dependent scattering of the Bloch waves at the ferromagnetic spacer-layer interface [7]. The interlayer exchange coupling was discovered in 1986 for Fe/Cr/Fe, Gd/Y/Gd, and Dy/Y/Dy structures [8–10]. This was followed by the discovery of the giant magnetoresistance effect in the interlayer exchanged-coupled Fe/Cr/Fe systems that gave birth to spin-dependent transport phenomena. Furthermore, interlayer exchange-coupled layers with a strong antiferromagnetic coupling in combination with an exchange-biased layer have also been extensively used as synthetic antiferromagnets in read head sensors in the magnetic recording industry. For the development of new magnetic recording technologies such as heat-assisted magnetic recording but also for the emerging spin-transfer-torque-based memories [11], obtaining a better understanding of the physical mechanisms that determine the temperature dependence of the interlayer exchange coupling remains an important goal.

Ferromagnetic resonance (FMR) is an excellent tool for quantitative determination of the interlayer exchange coupling for both ferromagnetically and antiferromagnetically coupled systems. Two different resonances are observed in the FMR spectra of the IEC structures [12,13]. For the acoustic mode, both layers precess in phase, whereas for the optic mode, they precess out of phase [11,12]. However, for two identical interlayer exchange-coupled ferromagnetic layers, the intensity of the optical mode is zero and, therefore, cannot be detected using FMR [14–16]. A common approach to circumvent this difficulty is, therefore, to use an asymmetric trilayer system, for example, by using ferromagnets with different film thicknesses. In this paper, we utilize broadband FMR to show that the mode separation used for experimental determination of the interlayer exchange coupling has a noticeable frequency dependence in asymmetric IEC systems where the two ferromagnetic layers are of different thicknesses. This frequency dependence arises from the difference in the effective magnetizations of the ferromagnetic layers [17]. Hence, for the experimental determination of the coupling strength, it is very important to have broadband ferromagnetic resonance data to avoid uncertainties for the interlayer exchange-coupling strength caused by the frequency dependence of the mode separation.

We perform a comprehensive experimental temperature-dependent investigation of the interlayer exchange-coupling strengths which enables us to compare them with the predictions of different theoretical models and thereby provides information about the physical origin of the temperature dependence.

II. EXPERIMENTAL PROCEDURES

The samples are fabricated using magnetron sputter deposition on SiO_2 substrates having the following layer sequence SiO_2/Ta(3 nm)/Ru(2 nm)/$Co_{90}Fe_{10}$(5 nm)/Ru(t)/$Co_{90}Fe_{10}$(8 nm)/Ru(3 nm)/Ta(3 nm)/Ru(3 nm). The thickness t of the Ru layer varies from 0.8 to 2.8 nm.

 © 2017 American Physical Society

The ferromagnetic resonance properties of the samples are measured using a custom designed broadband ferromagnetic resonance setup which uses a coplanar waveguide for microwave excitation and operates in the (1–65)-GHz frequency range [18–22]. At a fixed microwave frequency, the external magnetic field is swept through the resonance field of the sample. The microwave loss at the resonance condition can be detected by measuring the transmitted microwave power through the sample. The setup is also used with a closed-cycle cryostat for temperature-dependent measurements [23].

III. MODEL

A. Determination of interlayer exchange-coupling field by ferromagnetic resonance

For a trilayer system of two ferromagnetic layers separated by a nonmagnetic spacer, the interlayer exchange coupling, also known as RKKY coupling, results in two resonance modes of the system referred to as the acoustic and optic modes [1,4]. The acoustic mode corresponds to the in-phase and the optic mode to the out-of-phase precession of the ferromagnetic layers; see Fig. 1. For a symmetric trilayer, Eq. (1) describes the resonance frequencies for the acoustic and optic modes

$$f = \gamma' \sqrt{(H_{\mathrm{res,ac}})(H_{\mathrm{res,ac}} + 4\pi M_{\mathrm{eff}})},$$
$$f = \gamma' \sqrt{(H_{\mathrm{res,op}} + 2H_{\mathrm{ex}})(H_{\mathrm{res,op}} + 2H_{\mathrm{ex}} + 4\pi M_{\mathrm{eff}})}. \quad (1)$$

Here, the external magnetic field is applied in the film plane, H_{ex} is the interlayer exchange-coupling field, and M_{eff} is the effective magnetization, which for a symmetric trilayer is identical for both layers. Because of the oscillating nature of the RKKY interaction, the coupling between the two ferromagnetic layers changes sign with changing interlayer thickness between ferromagnetic $H_{\mathrm{ex}} > 0$ and antiferromagnetic $H_{\mathrm{ex}} < 0$. As seen in Eq. (1), the optic mode is shifted along the field axis by twice the exchange field as compared to the acoustic mode. Moreover, the resonance condition for the acoustic mode is identical to the resonance condition for a single-layer thin film. Therefore, in a symmetric trilayer structure, the exchange field is equal to half of the field separation between the two modes. However, in a typical ferromagnetic resonance measurement, the microwave magnetic field profile is homogeneous over the thin-film structure; hence, it is difficult to excite the optic mode in a symmetric trilayer [24]. One approach to overcome this difficulty is to use asymmetric trilayers, i.e., two ferromagnetic layers of different thicknesses, or different saturation magnetizations. In this case, solving the LLG equation leads to a more complicated dispersion relation as compared to the symmetric case.

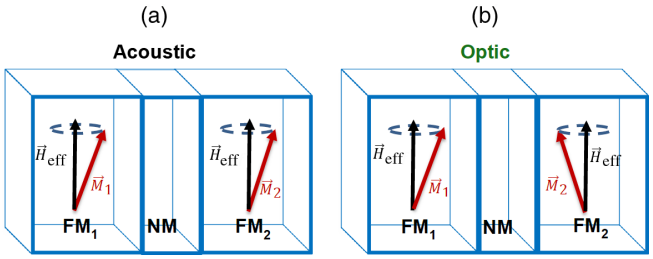

FIG. 1. Schematic diagram showing (a) the acoustic (in-phase) and (b) the optic (out-of-phase) FMR modes in an interlayer exchange-coupled trilayer. For the FM (AFM) coupling, the optic mode has a higher (lower) energy due to the exchange interaction. FM$_1$ and FM$_2$ stand for the two ferromagnetic layers and NM represents the nonmagnetic spacer layer. $\vec{M}_1$ and $\vec{M}_2$ indicate the magnetization vectors of the two ferromagnetic layers, and $\vec{H}_{\mathrm{eff}}$ is the effective static magnetic field.

Following the work of Zhang *et al.* [13], we use the following expression for the free-energy density of an asymmetric exchange-coupled trilayer:

$$E = \sum_{i=1}^{2} t_i[-M_s H_0(\cos\theta_H \cos\theta_i + \sin\theta_H \sin\theta_i \cos\varphi_i) - \frac{1}{2} 4\pi M_{\mathrm{eff},i} M_s \sin^2\theta_i] + J_{\mathrm{inter}}[\cos\theta_1 \cos\theta_2 + \sin\theta_1 \sin\theta_2 \cos(\varphi_1 - \varphi_2)]. \quad (2)$$

Here, θ_i and φ_i are the polar and azimuthal angles of the magnetization vectors of the ferromagnetic layers at equilibrium; see Fig. 2. Also, θ_H is the polar angle of the external magnetic field, which is $\theta_H = \pi/2$ in our configuration; see Fig. 2. Furthermore, J_{inter} is the effective coupling constant with units of energy per area, and $4\pi M_{\mathrm{eff},i}$ includes both demagnetization and perpendicular anisotropy fields and is defined as [19,23,25]

$$4\pi M_{\mathrm{eff},i} = 4\pi M_s - 2\frac{K_{u,i}}{M_s}, \quad (3)$$

where $K_{u,i}$ is the out-of-plane anisotropy constant. Here, $K_{u,i} > 0$ indicates that the easy axis of the perpendicular

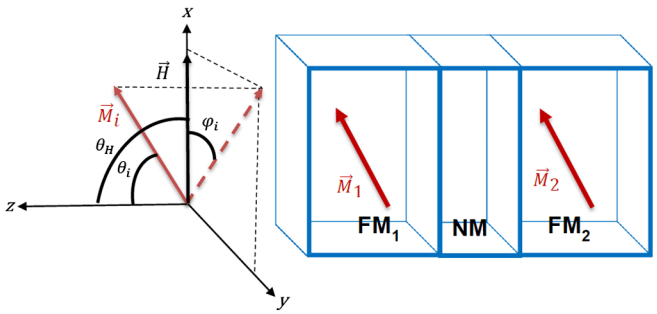

FIG. 2. The geometry of the interlayer exchange-coupled structure used for the numerical simulations. The z axis is normal to the thin-film structure, while the static magnetic field is applied in the film plane of the trilayer along the x direction.

magnetic anisotropy energy is along the film normal, whereas $K_{u,i} < 0$ corresponds to an easy plane in the film plane. In the case of thin films with no bulk contribution to the out-of-plane anisotropy, one has $K_{u,i} = (2k_i/t_i)$, where k_i is the average interfacial perpendicular anisotropy of layer i and t_i is its thickness. Therefore, the value of $K_{u,i}$ will generally be different for two ferromagnetic (FM) layers of different thicknesses. Note that no higher-order out-of-plane anisotropy or in-plane magnetic anisotropy fields are included in Eq. (2). Using the above energy density, the resonance frequencies of the acoustic and optic modes are found by solving the following equation

$$\left(\frac{f}{\gamma'}\right)^4 - b\left(\frac{f}{\gamma'}\right)^2 + c = 0, \tag{4}$$

where b and c are defined as follows [13]:

$$b = \frac{E_{\theta_1\theta_1}E_{\varphi_1\varphi_1} - {E_{\theta_1\varphi_1}}^2}{t_1^2 M_s^2 \sin^2\theta_1}\frac{E_{\theta_2\theta_2}E_{\varphi_2\varphi_2} - {E_{\theta_2\varphi_2}}^2}{t_2^2 M_s^2 \sin^2\theta_2} + 2\frac{E_{\theta_1\theta_2}E_{\varphi_1\varphi_2} - E_{\theta_1\varphi_2}E_{\theta_2\varphi_1}}{t_1 t_2 M_s^2 \sin\theta_1 \sin\theta_2},$$

$$\begin{aligned} c = \frac{1}{t_1^2 t_2^2 M_s^4 \sin^2\theta_1 \sin^2\theta_2}[&{E_{\theta_1\theta_2}}^2{E_{\varphi_1\varphi_2}}^2 + {E_{\theta_1\varphi_1}}^2{E_{\theta_2\varphi_2}}^2 + {E_{\theta_1\varphi_2}}^2{E_{\theta_2\varphi_1}}^2 - {E_{\theta_1\theta_2}}^2 E_{\varphi_1\varphi_1}E_{\varphi_2\varphi_2} - {E_{\varphi_1\varphi_2}}^2 E_{\theta_1\theta_1}E_{\theta_2\theta_2} \\ &- {E_{\theta_1\varphi_1}}^2 E_{\theta_2\theta_2}E_{\varphi_2\varphi_2} - {E_{\theta_1\varphi_2}}^2 E_{\theta_2\theta_2}E_{\varphi_2\varphi_2} - {E_{\theta_2\varphi_1}}^2 E_{\theta_1\theta_1}E_{\varphi_1\varphi_1} + E_{\theta_1\theta_1}E_{\varphi_1\varphi_1}E_{\theta_2\theta_2}E_{\varphi_2\varphi_2} + 2E_{\theta_1\theta_1}E_{\varphi_1\varphi_2}E_{\theta_2\varphi_2}E_{\theta_2\varphi_2} \\ &+ 2E_{\theta_1\varphi_1}E_{\theta_1\varphi_2}E_{\varphi_1\varphi_2}E_{\theta_2\theta_2} + 2E_{\theta_1\theta_2}E_{\theta_1\varphi_2}E_{\varphi_1\varphi_2}E_{\theta_2\varphi_2} + 2E_{\theta_1\theta_2}E_{\theta_1\varphi_1}E_{\theta_2\varphi_1}E_{\varphi_2\varphi_2} - 2E_{\theta_1\varphi_1}E_{\theta_2\varphi_2}(E_{\theta_1\theta_2}E_{\varphi_1\varphi_2} + E_{\theta_1\varphi_2}E_{\theta_2\varphi_1}) \\ &- 2E_{\theta_1\theta_2}E_{\varphi_1\varphi_2}E_{\theta_1\varphi_2}E_{\theta_2\varphi_1}], \end{aligned} \tag{5}$$

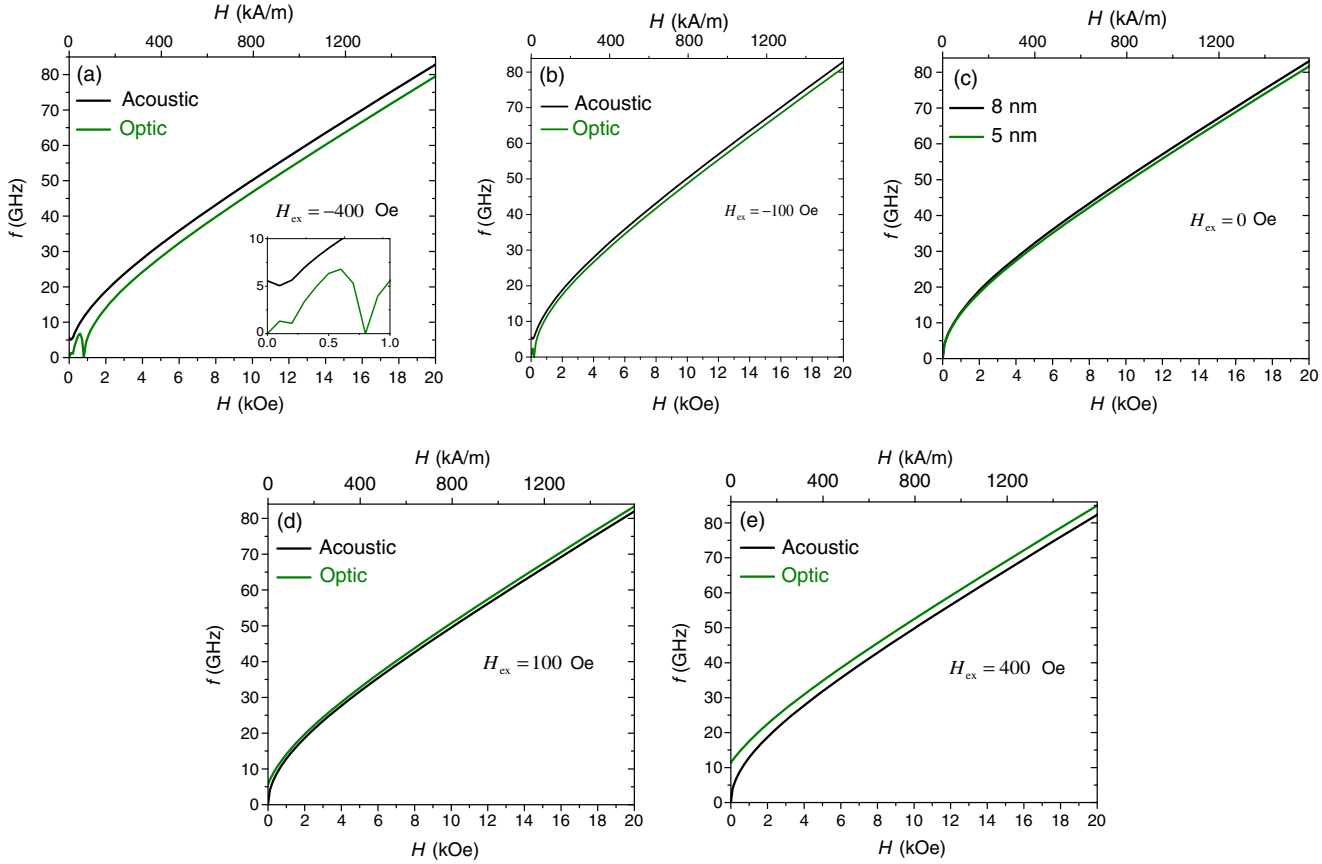

FIG. 3. Simulated Kittel plots based on Eq. (2) with an assumption of M_{eff} of 1300 emu/cm^3 and 1400 emu/cm^3 for a trilayer with 5- and 8-nm-thick Co-Fe layers. The exchange field is set to (a) $H_{\text{ex}} = -400$ Oe, (b) $H_{\text{ex}} = -100$ Oe, (c) $H_{\text{ex}} = 0$ Oe, (d) $H_{\text{ex}} = 100$ Oe, and (e) $H_{\text{ex}} = 400$ Oe. A negative sign corresponds to an antiferromagnetic coupling. The deviations observed in the resonance position of the optic and acoustic modes at low frequencies for the AFM coupled samples indicate that the samples are not saturated as the external magnetic field is not large enough to overcome the antiferromagnetic interlayer exchange coupling; see (a) and its inset.

where $E_{\theta\varphi}$ are the partial derivatives of the free-energy density E with respect to the magnetization angles at equilibrium, and M_s is the saturation magnetization, which for simplicity is assumed to be the same for the two layers.

B. Temperature dependence of the coupling field

While the origin of the interlayer exchange coupling has been studied in detail and is considered to be well understood [4,7,8], the origin of its temperature dependence remains an open question [26–29]. Here, we briefly summarize the theoretical mechanisms that have been proposed in the literature to explain the reduction of the interlayer exchange coupling at finite temperature. A detailed discussion can be found in the work by Schwieger *et al.* [26] and Schwieger and Nolting [27].

1. Spacer contribution and interface contributions

As proposed by Bruno [5,7], Bruno and Chappert [30], and Edwards *et al.* [31], the broadening of the Fermi edge in the spacer layer leads to a temperature dependence of the interlayer exchange coupling.

Furthermore, the phase and magnitude of the complex reflection coefficients at the interface between the ferromagnet and the spacer layer may also be temperature dependent.

The temperature dependence of the interlayer exchange coupling resulting from the spacer and interface contribution can be written as [27]

$$\tilde{J}_{\text{inter}} = \sum_{\alpha} \tilde{J}^{\alpha}_{\text{inter}}(t, T=0) f^{\alpha}(d, T), \tag{6}$$

where α counts the number of stationary Fermi-surface vectors relevant for the interlayer exchange coupling [30,32], and t is the spacer-layer thickness. Note that similar to the notation in Ref. [27], $\tilde{J}_{\text{inter}}$ in Eq. (6) has units of energy. The temperature-dependent functions are

$$f^{\alpha} = \frac{c_{\alpha} T}{\sinh(c_{\alpha} T)}, \tag{7}$$

where

$$c_{\alpha} = \frac{2\pi k_B}{\hbar v_f^{\alpha}} d + 2\pi k_B D_{\phi}^{\alpha}. \tag{8}$$

Here, the first and second terms on the rhs of Eq. (8) represent the spacer and interface contributions, respectively, also v_f^{α} is the Fermi velocity and $D_{\phi}^{\alpha} = [(d\phi^{\alpha})/(d\varepsilon)]_{\varepsilon=\varepsilon_f}$, where ϕ^{α} is the phase of reflection coefficient $\Delta r^{\alpha} = |r^{\alpha}| e^{i\phi\alpha}$. For the interlayer exchange coupling determined by a single Fermi-surface vector, one has

$$\frac{\tilde{J}_{\text{inter}}(T)}{\tilde{J}_{\text{inter}}(0)} = \frac{cT}{\sinh(cT)}. \tag{9}$$

2 Spin-wave excitations

Another mechanism that can contribute to the temperature dependence of the interlayer exchange interaction is spin-wave excitations in the magnetic layers [17,26,27,33]

$$\frac{\tilde{J}_{\text{inter}}(T)}{\tilde{J}_{\text{inter}}(0)} = 1 - \frac{1}{8\pi J S^2 \tilde{J}_{\text{inter}}(0)} (k_B T)^2 \sum(T),$$

$$\sum(T) = \sum_{n=1}^{\infty} \frac{1}{n^2} e^{-\beta g \mu_B B n} \left(1 - e^{-\frac{1}{S}\tilde{J}_{\text{inter}}(0)\beta n}\right),$$

$$\text{where } \beta = \frac{S}{k_B T}, \tag{10}$$

where S is the spin quantum number, and B is the magnetic induction. Note that J, which appears in the denominator of the first part of Eq. (10), denotes the intralayer exchange-coupling constant [27]. According to Eq. (10), the interlayer exchange coupling is expected to decrease with

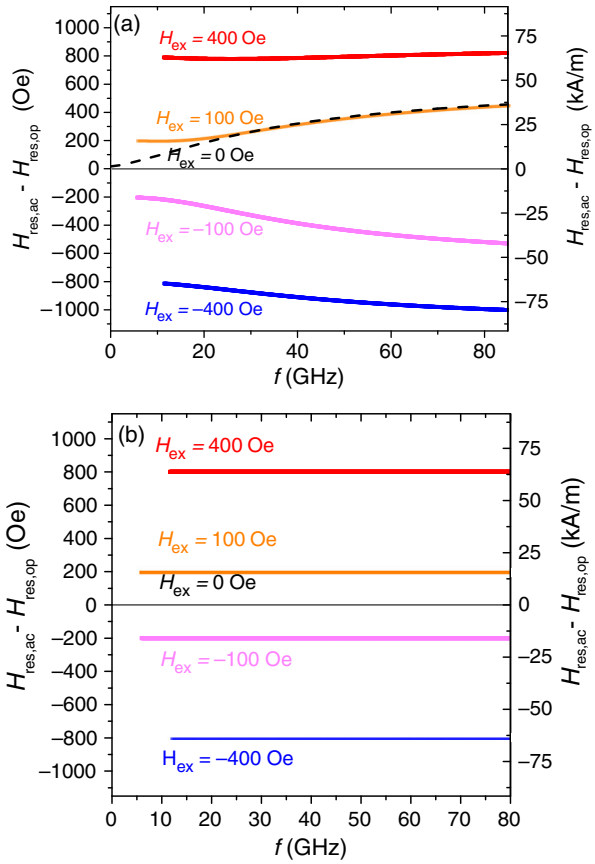

FIG. 4. Simulated frequency dependence of the mode separation $H_{\text{res,ac}} - H_{\text{res,op}}$ based on Eq. (2) with an assumption of (a) M_{eff} of 1300 emu/cm^3 and 1400 emu/cm^3 for a trilayer with 5- and 8-nm-thick Co-Fe layers for different coupling fields. The dashed line represents the zero-coupling case, and, therefore, the two resonances are simply the normal FMR modes of each layer. (b) shows that the frequency dependence of the mode separation disappears when identical effective magnetizations M_{eff} of 1400 emu/cm^3 for both 5- and 8-nm Co-Fe layers are assumed.

temperature faster than $1 - xT$ but slower than $1 - xT^2$; see Ref. [27].

As pointed out by Schwieger and Nolting [27], over the experimentally accessible temperature range, all three mechanisms can be approximated as

$$f(T) = \frac{\tilde{J}_{\text{inter}}(T)}{\tilde{J}_{\text{inter}}(0)} \approx 1 - xT^y, \qquad 1 < y < 2, \quad (11)$$

where the exponent y is expected to be in the range of 1 to 2 and is often assumed to be 1.5 [18–21]. The fact that all three contributions can be approximated by this power law explains the difficulty in distinguishing them solely based on the temperature dependence of the interlayer exchange coupling. However, the dependence of $f(T)$ on the spacer thickness can provide valuable insights. For the spacer contribution, one expects a linear increase of the parameter c in Eq. (8) with the spacer thickness t. The interface contribution, on the other hand, is independent of the spacer thickness; see Eq. (8). The contribution due to the spin-wave excitations shows a weak implicit dependence that oscillates with the spacer thickness [26,27]. This model predicts a more pronounced temperature dependence for small coupling fields.

IV. NUMERICAL RESULTS

Equation (4) is solved numerically in the (0–20)-kOe interval to determine the resonance frequencies of both acoustic and optic modes at each magnetic field point for an asymmetric IEC trilayer. The gyromagnetic ratio γ' is 3.03 GHz/kOe for both layers, and the effective magnetization M_{eff} is set to 1300 and 1400 emu/cm^3 for the 5- and 8-nm Co-Fe layers, respectively. These parameters are selected in light of the experimental values of the gyromagnetic ratio and effective magnetization for a Co-Fe

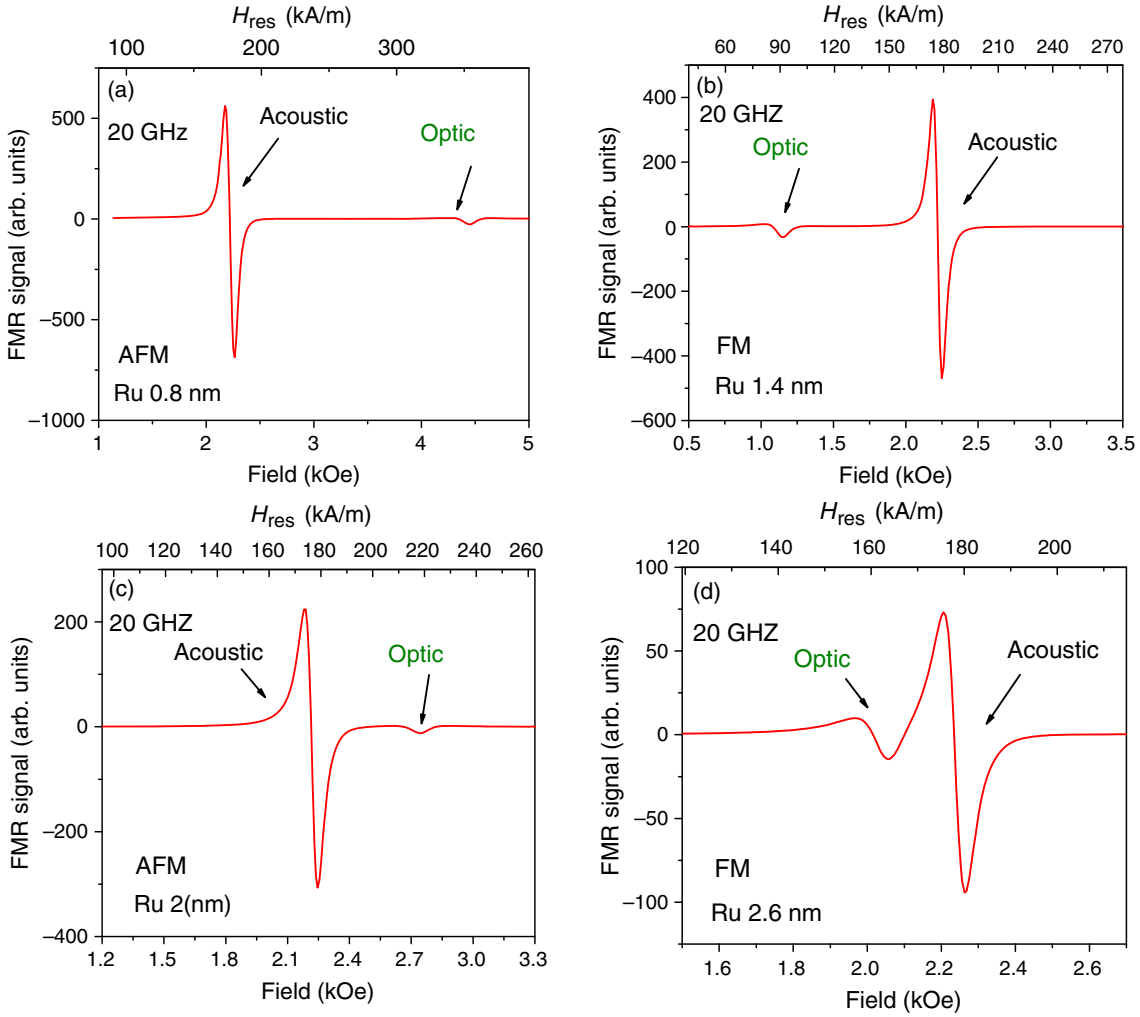

FIG. 5. (a),(c) Raw FMR spectra for the Co-Fe(5 nm)/Ru(0.8 nm)/Co-Fe(8 nm) and Co-Fe(5 nm)/Ru(2 nm)/Co-Fe(8 nm) AFM coupled samples. (b),(d) Raw FMR spectra for the Co-Fe(5 nm)/Ru(1.4 nm)/Co-Fe(8 nm) and Co-Fe(5 nm)/Ru(2.6 nm)/Co-Fe(8 nm) FM coupled samples. Note that the optic mode appears on the low-field side of the acoustic mode for the ferromagnetic coupling and on the high-field side for the antiferromagnetic coupling.

(13 nm) single layer, which are equal to 3.03 GHz/kOe and 1420 emu/cm^3, respectively; see Sec. V. The simulated frequency versus resonance field plots are shown in Fig. 3 for coupling field values of −400 Oe (a), −100 Oe (b), 0 Oe (c), 100 Oe (d), and 400 Oe (e), where the negative sign refers to antiferromagnetic coupling. Note that for simplicity, the saturation magnetization of both layers is assumed to be the same value, but a small interfacial perpendicular magnetic anisotropy is assumed, which leads to the different effective magnetization values for the 5-nm (1300 emu/cm^3) and 8-nm Co-Fe (1400 emu/cm^3). We point out that for asymmetric trilayers, we define the interlayer exchange-coupling field as [13]

$$H_{\mathrm{ex}} = \frac{1}{2}\frac{(t_1 + t_2)J_{\mathrm{inter}}}{M_s t_1 t_2}; \tag{12}$$

i.e., the effective interlayer exchange field is equal to the arithmetic mean of the exchange field values for each FM layer, $H_{\mathrm{ex},i} = (J_{12}/M_s t_i)$. Figure 4(a) shows the frequency dependence of the field separation between the acoustic and optic modes that is found from the numerical frequency versus resonance field plots shown in Fig. 3. As can be expected, the difference of the effective magnetizations of the two layers leads to a frequency dependence of the mode separation. As shown in Fig. 4(b), this frequency dependence of the mode separation vanishes for two FM layers with equal effective magnetization. Therefore, broadband ferromagnetic resonance measurements are required to reliably extract the interlayer exchange coupling of the trilayers for which the assumption of equal effective magnetizations cannot be supported using independent measurements. As we show below, the fitting of broadband

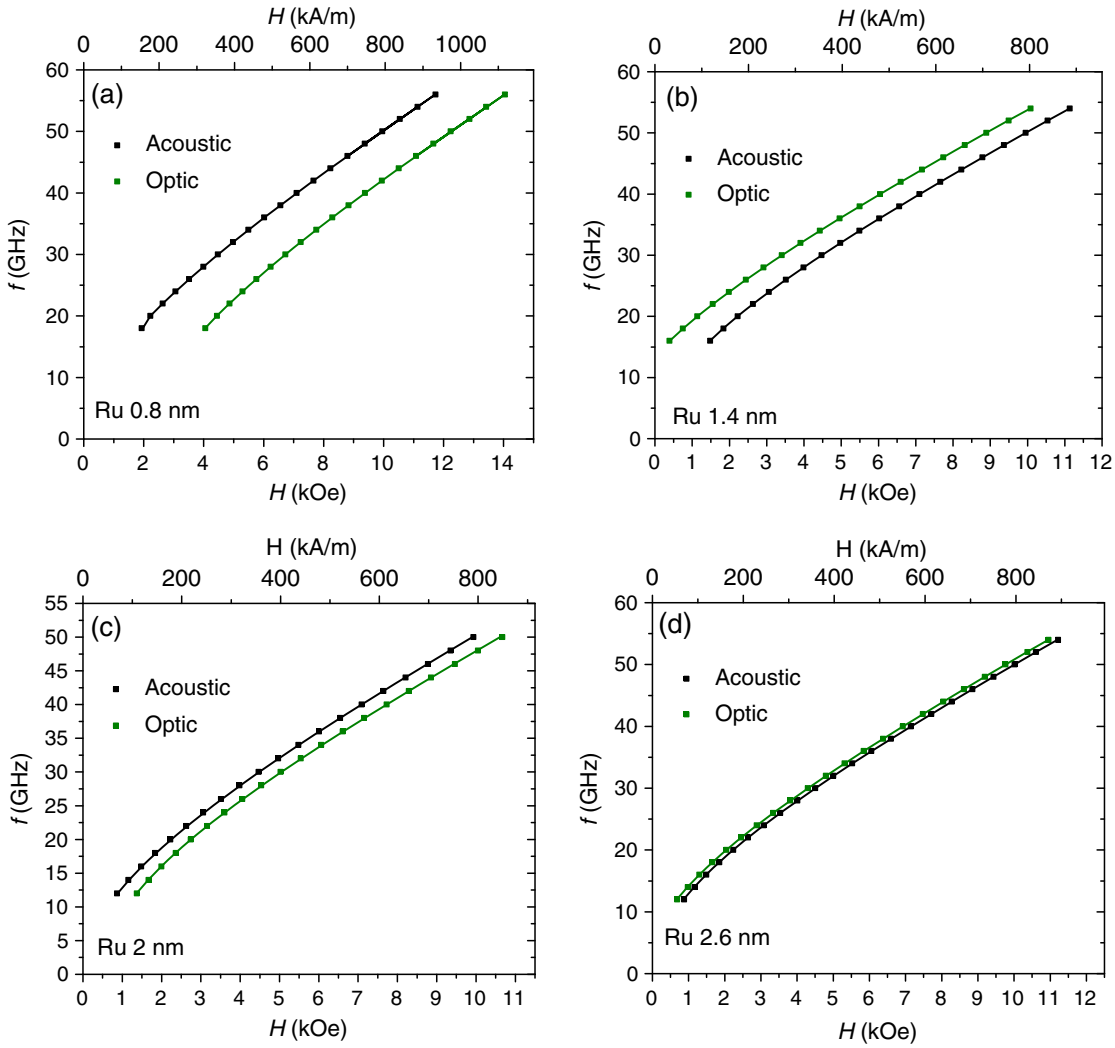

FIG. 6. (a),(c) Plots of ferromagnetic resonance frequency as a function of resonance field (Kittel plots) for the Co-Fe(5 nm)/Ru(0.8 nm)/Co-Fe(8 nm) and Co-Fe(5 nm)/Ru(2 nm)/Co-Fe(8 nm) AFM coupled samples. (b),(d) Kittel plots for the Co-Fe(5 nm)/Ru(1.4 nm)/Co-Fe(8 nm) and Co-Fe(5 nm)/Ru(2.6 nm)/Co-Fe(8 nm) FM coupled samples. The data in black color correspond to the acoustic mode, and green corresponds to the optic mode. The symbols represent the experimental data, and the lines are the fits to the experimental data using the full numerical model; see Eq. (4).

FMR data enables the precise determination of the interlayer exchange coupling and the effective magnetizations of the trilayers.

V. EXPERIMENTAL RESULTS

A. Frequency dependence of the mode separation

Figure 5 shows the experimental raw FMR signals at 20 GHz for the Co-Fe(5 nm)/Ru(0.8 nm)/Co-Fe(8 nm) [Fig. 5(a)] and Co-Fe(5 nm)/Ru(2 nm)/Co-Fe(8 nm) [Fig. 5(c)] samples with antiferromagnetic interlayer exchange coupling and Co-Fe(5 nm)/Ru(1.4 nm)/Co-Fe(8 nm) [Fig. 5(b)] and Co-Fe(5 nm)/Ru(2.6 nm)/Co-Fe(8 nm) [Fig. 5(d)] samples, which show ferromagnetic interlayer exchange coupling.

Figure 6 shows the broadband experimental Kittel plots for the same samples as in Fig. 5, which enables us to determine the $H_{\mathrm{res,ac}} - H_{\mathrm{res,op}}$ between the acoustic and optic modes.

As shown in Fig. 7 the experimental field separation data show the same trend as a function of frequency as the numerical simulations discussed in the previous section. In order to accurately determine the coupling field, the experimental H_{res} versus frequency data for both modes are fitted with the full numerical model using Eq. (2) as shown in Figs. 6(a)–6(d) and 7 for exemplary antiferromagnetic (AFM) and FM coupled samples. This approach minimizes systematic errors caused by the frequency dependence of the mode separation and is used to determine the experimental value of the interlayer exchange-coupling field H_{ex} for all samples. As an example to illustrate this, consider the Co-Fe(5 nm)/Ru(2 nm)/Co-Fe(8 nm) sample. Here, the fit using the full model results in an interlayer exchange-coupling field of $H_{\mathrm{ex}} = -250 \pm 3$ Oe. If one instead uses half the field separation of the two resonances at 50 GHz, as implied by Eq. (1), then one obtains a value for the interlayer exchange-coupling field of $H_{\mathrm{ex}} = -367$ Oe. This value differs by almost 47% from the value determined using the full model. Because this approach takes into account data collected over a wide frequency range, the error margins are very small; see Fig. 7. Determining meaningful error margins for the interlayer exchange field determined from the field separation at a single frequency is also challenging. When fitting broadband data using the full model, on the other hand, one can determine the statistical error margins by calculating the approximation of the Hessian matrix and its inverse at the convergence point [34].

To conclude, we show that in asymmetric trilayers, the interlayer exchange coupling is not solely responsible for the field separation between the optic and acoustic modes, as differences between the effective magnetizations of the ferromagnetic layers also influence the mode separation.

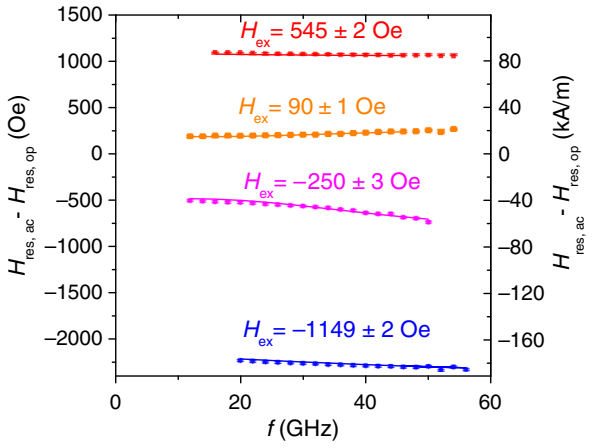

FIG. 7. Frequency dependence of the mode separation $H_{\mathrm{res,ac}} - H_{\mathrm{res,op}}$ for the Co-Fe(5 nm)/Ru(0.8 nm)/Co-Fe(8 nm) (blue), Co-Fe(5 nm)/Ru(2 nm)/Co-Fe(8 nm) (magenta) AFM coupled samples and Co-Fe(5 nm)/Ru(1.4 nm)/Co-Fe(8 nm) (red) and Co-Fe(5 nm)/Ru(2.6 nm)/Co-Fe(8 nm) (orange) FM coupled samples. The symbols represent the experimental data, and the lines show the full numerical fit to the experimental data using the full model; see Eq. (4).

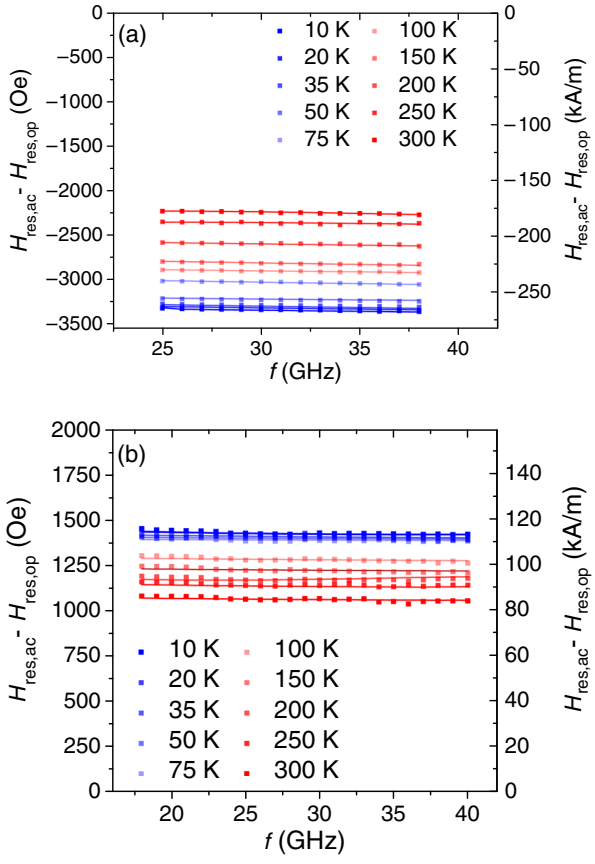

FIG. 8. Frequency dependence of the mode separation $H_{\mathrm{res,ac}} - H_{\mathrm{res,op}}$ for the (a) Co-Fe(5 nm)/Ru(0.8 nm)/Co-Fe(8 nm) and (b) Co-Fe(5 nm)/Ru(1.4 nm)/Co-Fe(8 nm) samples, as a function of the temperature. The symbols represent the experimental data, and the lines show the full numerical fit to the experimental data using the full model; see Eq. (4).

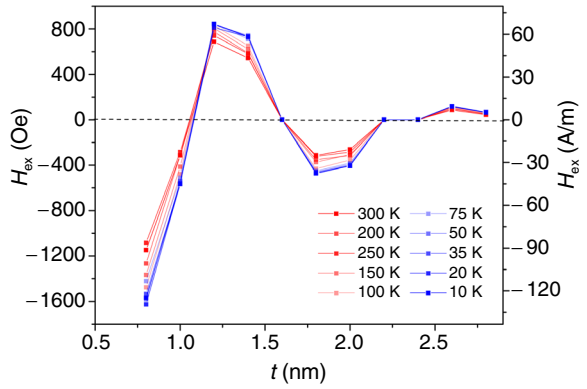

FIG. 9. Interlayer exchange-coupling field H_{ex} of the Co-Fe/Ru/Co-Fe interlayer exchange-coupled system as a function of Ru thickness from room temperature down to 10 K. The $t_{Ru} = 2.2$ nm and $t_{Ru} = 2.4$ nm data correspond to the samples where the optic and acoustic signals are merged together due to a very weak coupling, therefore, preventing the determination of the interlayer exchange-coupling field, which in these cases, is set to zero.

Broadband measurements enable us to identify and distinguish between these two contributions.

B. Temperature dependence of the coupling field

In addition to the room-temperature experiments, a comprehensive set of broadband ferromagnetic resonance measurements are performed at lower temperatures down to 10 K.

Figure 8 shows exemplary experimental broadband temperature-dependent data for the samples with Ru thicknesses of 0.8 and 1.2 nm. The data are fitted using the full numerical model to determine the interlayer exchange-coupling field at each temperature. Figure 9 shows the experimentally determined interlayer exchange-coupling field as a function of Ru thickness at different temperatures. The strongest antiferromagnetic coupling is observed for the sample with the smallest Ru thickness of 0.8 nm, and the first transition from antiferromagnetic coupling to ferromagnetic coupling happens between 1 and 1.2 nm and the second transition from AFM to FM coupling takes place

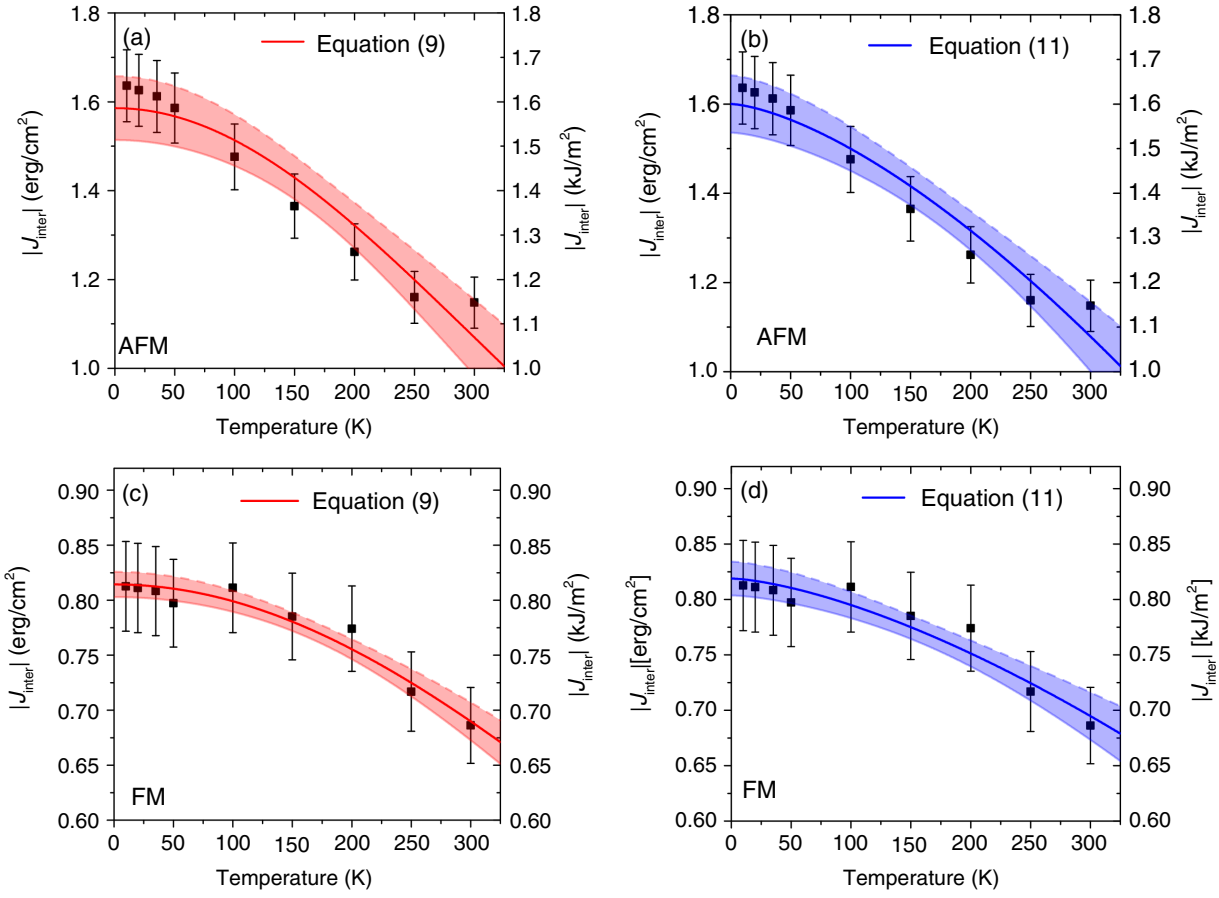

FIG. 10. Temperature dependence of the absolute value of the interlayer exchange-coupling constant J_{inter} for the Co-Fe(5 nm)/Ru(0.8 nm)/Co-Fe(8 nm) (a),(b) and Co-Fe(5 nm)/Ru(1.2 nm)/Co-Fe(8 nm) samples (c),(d). The experimental data are represented by symbols; the blue line is a fit to the data using Eq. (11) with a fixed value of $y = 1.5$, whereas the red line is a fit using Eq. (9). Both fits are weighted with the standard deviation of the individual data points, and confidence bands are shown as shaded areas.

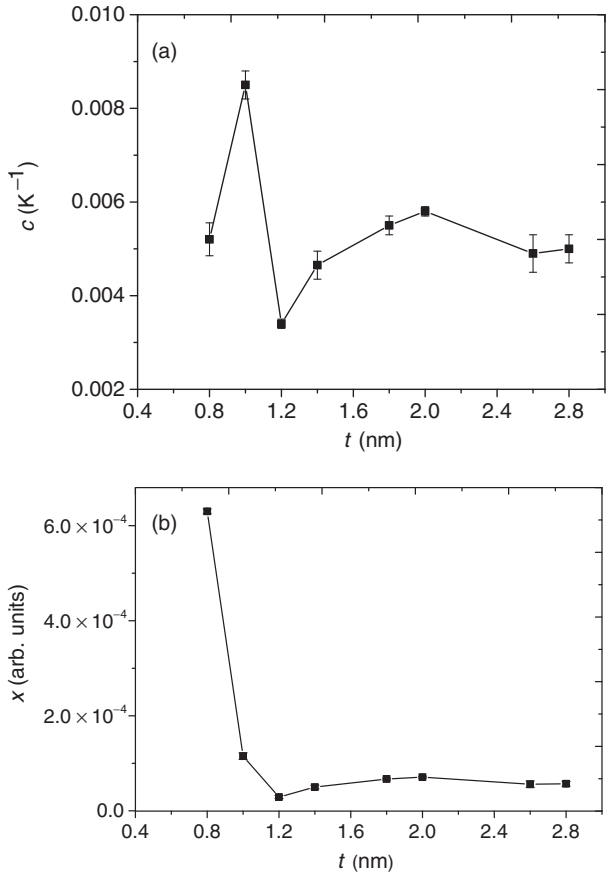

FIG. 11. (a) Fit parameter c of the spacer and interface model described by Eq. (9) as a function of Ru thickness. (b) The fit parameter x of Eq. (11) as a function of Ru thickness.

between 2 and 2.4 nm. The strongest ferromagnetic coupling is observed at a thickness of 1.2 nm with the second antiferromagnetic and ferromagnetic peaks occurring at 1.8 and 2 nm, respectively, and the coupling crossover from ferromagnetic to antiferromagnetic happening between 1.4 and 1.8 nm. In accordance with all three theoretical models, the oscillation amplitude (coupling field) increases noticeably with decreasing temperature, while the oscillation period remains unchanged [13,30]. The period of oscillation is approximately 1.1 nm, which is consistent with the reported value for Co/Ru superlattice structures [35].

In order to compare our experimental results with the theoretical predictions for the temperature dependence discussed in Sec. III B, we determine the interlayer exchange-coupling constant J_{inter} using Eq. (12). Here, we use $M_s = 1600$ emu/cm^3 for all temperatures, as the changes in M_s are expected to be small in accessible temperature range. Note that the Curie temperature of Co-Fe alloys is very high, close to 1000 °C [36,37].

Figure 10 shows the temperature dependence of the coupling constant for the samples with Ru thicknesses of 0.8 and 1.2 nm and the fits to the experimental data using Eqs. (9) and (11). Note that the uncertainties of the coupling constant J_{inter} values are calculated using Eq. (12) and the standard deviations of the numerically fitted values of H_{ex}, while considering a 5% error margin in the values of saturation magnetization and thicknesses of the Co-Fe layers. As shown in Fig. 10, both Eqs. (9) and (11) result in a reasonable agreement with the experimental data and a similar fit quality.

As we discuss in Sec. III, despite the difficulties in distinguishing between the existing theoretical models caused by their similar temperature dependence, one can obtain further insights by investigating the influence of the spacer-layer thickness, magnitude, and sign of the interlayer exchange coupling on the temperature dependence of the model parameters. When comparing the spacer and interface models as described by Eq. (9) and the more generally applicable approximation given by Eq. (11), one notes that the fit parameter x is highly correlated to fit parameter c [27], which itself is supposed to scale linearly with the spacer-layer thickness based on the spacer model; see Eq. (8). As shown in Fig. 11, no such dependence is seen for the fit parameters c or x. On the other hand, the oscillatory behavior of both fit parameters, which is more pronounced in the case of the c parameter, follows the oscillatory behavior of the exchange field as a function of the spacer-layer thickness, which is consistent with the prediction of the spin-wave excitation model.

VI. CONCLUSION

In summary, a frequency dependence is found in the FMR mode separation of asymmetric interlayer exchange-coupled Co-Fe/Ru/Co-Fe trilayers. Our numerical simulations confirm that this frequency dependence stems from the difference between the effective magnetizations of the two magnetic layers. The systematic uncertainties in the experimental determination of the interlayer exchange-coupling field caused by this frequency dependence are minimized by fitting broadband experimental FMR data using the full numerical model. A comparison of the comprehensive temperature-dependent results with the existing theoretical models reveals that the thermal spin-wave model shows a better agreement with the experimental data.

ACKNOWLEDGMENTS

We acknowledge support by National Science Foundation Faculty Early Career Development Program (NSF-CAREER) Grants No. 0952929 and No. 1452670.

[1] A. Layadi and J. O. Artman, Effect of biquadratic coupling and in-plane anisotropy on the resonance modes of a trilayer system, J. Magn. Magn. Mater. **92**, 143 (1990).

[2] S. M. Rezende, C. Chesman, M. A. Lucena, A. Azevedo, F. M. de Aguiar, and S. S. P. Parkin, Studies of coupled

metallic magnetic thin-film trilayers, J. Appl. Phys. **84**, 958 (1998).
[3] Z. Zhang, P. E. Wigen, and K. Ounadjela, FMR in strongly coupled Co/Ru/Co structures, IEEE Trans. Magn. **29**, 2717 (1993).
[4] M. D. Stiles, Interlayer exchange coupling, J. Magn. Magn. Mater. **200**, 322 (1999).
[5] P. Bruno, Theory of interlayer magnetic coupling, Phys. Rev. B **52**, 411 (1995).
[6] M. A. Ruderman and C. Kittel, Indirect exchange coupling of nuclear magnetic moments by conduction electrons, Phys. Rev. **96**, 99 (1954).
[7] P. Bruno, Theory of interlayer exchange interactions in magnetic multilayers, J. Phys. Condens. Matter **11**, 9403 (1999).
[8] P. Grünberg, R. Schreiber, Y. Pang, M. B. Brodsky, and H. Sowers, Layered Magnetic Structures: Evidence for Antiferromagnetic Coupling of Fe Layers across Cr Interlayers, Phys. Rev. Lett. **57**, 2442 (1986).
[9] C. F. Majkrzak, J. W. Cable, J. Kwo, M. Hong, D. B. McWhan, Y. Yafet, J. V. Waszczak, and C. Vettier, Observation of a Magnetic Antiphase Domain Structure with Long-Range Order in a Synthetic Gd-Y Superlattice, Phys. Rev. Lett. **56**, 2700 (1986).
[10] M. B. Salamon, S. Sinha, J. J. Rhyne, J. E. Cunningham, R. W. Erwin, J. Borchers, and C. P. Flynn, Long-Range Incommensurate Magnetic Order in a Dy-Y Multilayer, Phys. Rev. Lett. **56**, 259 (1986).
[11] E. Chen *et al.*, Progress and prospects of spin transfer torque random access memory, IEEE Trans. Magn. **48**, 3025 (2012).
[12] M. N. Baibich, J. M. Broto, A. Fert, F. N. Van Dau, F. Petroff, P. Etienne, G. Creuzet, A. Friederich, and J. Chazelas, Giant Magnetoresistance of (001)Fe/(001)Cr Magnetic Superlattices, Phys. Rev. Lett. **61**, 2472 (1988).
[13] Z. Zhang, L. Zhou, P. E. Wigen, and K. Ounadjela, Angular dependence of ferromagnetic resonance in exchange-coupled Co/Ru/Co trilayer structures, Phys. Rev. B **50**, 6094 (1994).
[14] B. Heinrich, Z. Celinski, J. F. Cochran, W. B. Muir, J. Rudd, Q. M. Zhong, A. S. Arrott, K. Myrtle, and J. Kirschner, Ferromagnetic and Antiferromagnetic Exchange Coupling in bcc Epitaxial Ultrathin Fe(001)/Cu(001)Fe(001) Trilayers, Phys. Rev. Lett. **64**, 673 (1990).
[15] B. Heinrich, S. T. Purcell, J. R. Dutcher, K. B. Urquhart, J. F. Cochran, and A. S. Arrott, Structural and magnetic properties of ultrathin Ni/Fe bilayers grown epitaxially on Ag(001), Phys. Rev. B **38**, 12879 (1988).
[16] A. Layadi, Effect of biquadratic coupling and in-plane anisotropy on the resonance modes of a trilayer system, Phys. Rev. B **65**, 104422 (2002).
[17] J. Lindner and K. Baberschke, *In situ* ferromagnetic resonance: An ultimate tool to investigate the coupling in ultrathin magnetic films, J. Phys. Condens. Matter **15**, R193 (2003).
[18] B. Khodadadi, Ph.D. thesis, The University of Alabama, 2016.
[19] Y. Cui, B. Khodadadi, S. Schäfer, T. Mewes, J. Lu, and S. A. Wolf, Interfacial perpendicular magnetic anisotropy and damping parameter in ultra thin Co_2FeAl films, Appl. Phys. Lett. **102**, 162403 (2013).
[20] S. Keshavarz, Y. Xu, S. Hrdy, C. Lemley, T. Mewes, and Y. Bao, Relaxation of polymer coated magnetic nanoparticles in aqueous solution, IEEE Trans. Magn. **46**, 1541 (2010).
[21] S. Klingler, A. V. Chumak, T. Mewes, B. Khodadadi, C. Mewes, C. Dubs, O. Surzhenko, B. Hillebrands, and A. Conca, Measurements of the exchange stiffness of YIG films using broadband ferromagnetic resonance techniques, J. Phys. D **48**, 015001 (2015).
[22] C. Sterwerf, S. Paul, B. Khodadadi, M. Meinert, J.-M. Schmalhorst, M. Buchmeier, C. K. A. Mewes, T. Mewes, and G. Reiss, Low Gilbert damping in Co_2FeSi and Fe_2CoSi films, J. Appl. Phys. **120**, 083904 (2016).
[23] N. Pachauri, B. Khodadadi, A. V. Singh, J. B. Mohammadi, R. L. Martens, P. R. LeClair, C. Mewes, T. Mewes, and A. Gupta, A comprehensive study of ferromagnetic resonance and structural properties of iron-rich nickel ferrite (NixFe3-xO$_4$, $x \leq 1$ films grown by chemical vapor deposition, J. Magn. Magn. Mater. **417**, 137 (2016).
[24] Z. Zhang, L. Zhou, P. E. Wigen, and K. Ounadjela, Using Ferromagnetic Resonance as a Sensitive Method to Study Temperature Dependence of Interlayer Exchange Coupling, Phys. Rev. Lett. **73**, 336 (1994).
[25] B. Heinrich, in *Ultrathin Magnetic Structures III: Fundamentals of Nanomagnetism*, edited by J. A. C. Bland and B. Heinrich (Springer, Berlin, 2005), pp. 143–210.
[26] S. Schwieger, J. Kienert, K. Lenz, J. Lindner, K. Baberschke, and W. Nolting, Spin-Wave Excitations: The Main Source of the Temperature Dependence of Interlayer Exchange Coupling in Nanostructures, Phys. Rev. Lett. **98**, 057205 (2007).
[27] S. Schwieger and W. Nolting, Origin of the temperature dependence of interlayer exchange coupling in metallic trilayers, Phys. Rev. B **69** (22), 224413 (2004).
[28] S. S. Kalarickal, X. Y. Xu, and K. Lenz, Dominant role of thermal magnon excitation in temperature dependence of interlayer exchange coupling: Experimental verification, Phys. Rev. B **75**, 224429 (2007).
[29] J. Lindner, C. Rüdt, E. Kosubek, P. Poulopoulos, K. Baberschke, P. Blomquist, R. Wäppling, and D. L. Mills, $T^{3/2}$ Dependence of the Interlayer Exchange Coupling in Ferromagnetic Multilayers, Phys. Rev. Lett. **88**, 167206 (2002).
[30] P. Bruno and C. Chappert, Oscillatory Coupling between Ferromagnetic Layers Separated by a Nonmagnetic Metal Spacer, Phys. Rev. Lett. **67**, 1602 (1991).
[31] D. M. Edwards, J. Mathon, R. B. Muniz, and M. S. Phan, Oscillations of the Exchange in Magnetic Multilayers as an Analog of de Haas–van Alphen Effect, Phys. Rev. Lett. **67**, 493 (1991).
[32] V. Drchal, J. Kudrnovský, P. Bruno, I. Turek, P. H. Dederichs, and P. Weinberger, Temperature dependence of the interlayer exchange coupling in magnetic multilayers: An *ab initio* approach, Phys. Rev. B **60**, 9588 (1999).
[33] K. Baberschke, Magnetic anisotropy energy and interlayer exchange coupling in ultrathin ferromagnets: Experiment versus theory, Philos. Mag. **88**, 2643 (2008).
[34] P. Richter, Estimating errors in least-squares fitting, TDA Prog. Rep. **42**, 107 (1995).

[35] S. S. P. Parkin, N. More, and K. P. Roche, Oscillations in Exchange Coupling and Magnetoresistance in Metallic Superlattice Structures: Co/Ru, Co/Cr, and Fe/Cr, Phys. Rev. Lett. **64**, 2304 (1990).

[36] C. H. Shang, T. P. Weihs, R. C. Cammarata, Y. Ji, and C. L. Chien, Anisotropy in magnetic and mechanical properties in textured Hiperco® FeCoV alloys, J. Appl. Phys. **87**, 6508 (2000).

[37] C.-H. Shang, R. C. Cammarata, T. P. Weihs, and C. L. Chien, Microstructure and Hall-Petch behavior of Fe-Co-based Hiperco© alloys, J. Mater. Res. **15**, 835 (2000).